scientific reports

Check for updates

OPEN

Effects of mass concentration and curing age on the mechanical properties and damage evolution of aeolian sand backfill

Guibin Zhao[1], Yafei Zhang[2]✉, Guangli Zhang[1], Hao Zhang[3] & Xiufeng Zhang[3]

As the critical load-bearing structure in the management of open-pit mine goaf areas, the mechanical properties of cemented backfill material play a decisive role in strata stability. This study investigates the influence of solids mass concentration (*α*) and curing age (*T*) on the mechanical response and damage evolution of aeolian sand backfill material through uniaxial compression tests, acoustic emission (AE) monitoring, and scanning electron microscopy (SEM) experiments. The results demonstrate that both the uniaxial compressive strength and elastic modulus of the backfill increase linearly with mass concentration and exhibit an exponential enhancement with increasing curing age. At *α* = 80% and *T* = 28 d, he uniaxial compressive strength and elastic modulus reach the maximum values of 7.01 MPa and 0.18 GPa, respectively. The microstructure analysis reveals that higher mass concentrations promote the formation of hydration products, reduce porosity, and lead to a more compact structure. Acoustic emission signals indicate that high-*α* specimens accumulate more energy prior to failure, and crack propagation becomes more localized and abrupt, exhibiting typical brittle failure characteristics. Energy evolution analysis further demonstrates that, with increasing *α*, the elastic strain energy ratio rises from 53.25 to 67.19%, while the dissipated energy ratio declines from 46.75 to 32.81%, reflecting enhanced structural homogeneity and improved interfacial bonding within the backfill. The findings provide a theoretical foundation and experimental support for the engineering application of aeolian sand backfill materials in open-pit mining.

Keywords Aeolian sand, Mass concentration, Curing age, Uniaxial compressive strength, Elastic modulus, Acoustic emission

Coal remains the dominant and critical primary energy source in China's energy structure[1,2]. By the end of 2024, China's coal production had reached 4.78 billion tons. Open-pit mines, which constituted approximately 8% of the number of coal mines, contributed about 23% of the country's coal production. As the scale of open-pit coal mining expands, goafs from earlier underground mining operations are progressively uncovered posing significant safety hazards to open-pit operations. Consequently, goaf management has become a critical component for ensuring the safety and sustainability of open-pit mining. Among existing treatment technologies, cemented backfilling has emerged as the mainstream approach due to its dual advantages of supporting surrounding rock and utilizing solid waste[3]. As the principal load-bearing structure in the management of open-pit mine goaf areas, the mechanical properties of cemented backfill material (a mixture of solid waste, binder, and water used to fill underground voids) have a decisive influence on the control effect of rock strata, and its mechanical performance is governed by mix proportions, curing age, and other factors. Therefore, investigating the mechanical properties and damage evolution of cemented backfill materials under different material proportions[4,5] and curing ages is crucial for ensuring mine safety and promoting friendly mining practices.

Traditional backfill aggregates, such as river sand[6] and tailings[7–9], face challenges including resource scarcity and environmental risks, necessitating the development of new alternative materials. Aeolian sand, widely available in north-western China, features abundant reserves, low cost, and environmental friendliness, making

[1]CHN Energy Baorixile Energy Co., Ltd., Hulunbuir 021000, China. [2]State Key Laboratory of Intelligent Construction and Healthy Operation and Maintenance of Deep Underground Engineering, China University of Mining and Technology, Xuzhou 221116, China. [3]Baorixile Open-pit Mine, CHN Energy Baorixile Energy Co., Ltd., Hulunbuir 021000, China. ✉email: yafeizhang@cumt.edu.cn

it an ideal choice for backfill material[10]. In recent years, scholars have conducted numerous studies on cemented backfill materials, leading to significant advances in the field of aeolian sand backfill. Regarding the rheological properties of backfill materials, Wang et al.[11] employed response-surface methodology to show that rheological parameters increase with ordinary Portland (PO) cement, the ratio of fly ash (FA) to aeolian sand (AS) and mass concentration, while the exudation rate first decreased and then increased with PO content. Xin et al.[12] observed that higher activator dosages increase the yield stress, apparent viscosity, thixotropy, and slump of aeolian sand-cement-modified gasification slag-paste backfill (ACGPB) pastes. Zhou et al.[13] demonstrated that higher contents of fly ash, cement, and lime slag, together with increased mass concentration, reduce bleeding and slump of the backfill slurry, whereas prolonged curing consistently improves mechanical performance. Additionally, Zhu et al.[14] reported that although the full aeolian sand concrete exhibited improved fluidity, its drying shrinkage and strength progressively decreased with increasing dosage, with a 42.4% reduction in the 3-day compressive strength. Zhao et al.[15] systematically evaluated the effects of water content, water type, and temperature on the rheological properties of cemented paste backfill (CPB) slurry, and elucidated the governing mechanisms of water content, temperature, and binder type on its rheological behavior. Wang et al.[16] integrated computational fluid dynamics (CFD) simulations with rheological testing, identifying slurry concentration, flow velocity, and pipe diameter as the core factors affecting pipeline pressure drop. This finding provides a basis for optimizing the energy-efficient design of transport systems. Regarding the mix design and performance optimization of materials, Xia et al.[17] combined field and laboratory tests to demonstrate that aeolian sand exhibits low moisture content, negligible cohesion and high compactibility, with bearing capacity governed by fines and water content. Following this, the magnesium slag-fly ash based aeolian sand backfill developed by Ruan et al.[18] and the novel paste backfill optimized from coal gangue, fly ash, aeolian sand, and loess by Zhang et al.[19] both demonstrated excellent long-term strength development. Wan et al.[20] further utilized lead smelting slag and aeolian sand to successfully fabricate an environmentally friendly backfill material featuring mechanical properties and effective heavy metal immobilization. The performance of cemented backfill is governed not only by its mix proportion, but also more profoundly regulated by the curing conditions and the resulting microstructure. Fall et al.[21] confirmed that curing temperature significantly affects backfill strength, with the magnitude of the effect modulated by cement type, water-binder ratio, and curing age. Zheng et al.[22] found that increasing the coal gangue particle size enhances the unconfined compressive strength, revealing the regulatory role of aggregate gradation. Wang et al.[23] demonstrated that the incorporation of fibers enhances freeze-thaw durability through the effective inhibition of crack growth, clarifying the underlying micro-mechanism. Simultaneously, Hefni[24] demonstrated that basalt fiber incorporation not only improves CPB performance but also offers a viable strategy for reducing cement usage and enhancing mechanical properties. Regarding mechanical behavior and damage evolution, Li et al.[25] found that the dynamic elastic modulus of aeolian sand concrete exhibits a non-monotonic trend (decreasing, then increasing, and then decreasing) with increasing content, while the porosity in a stress-free state shows an oscillatory behavior. Hou et al.[26] revealed that characteristic stresses of cemented tailings backfill scale exponentially with curing age, and proposed a failure criterion based on the elastic energy dissipation ratio. Shao et al.[27] demonstrated that higher loading rates markedly improve the uniaxial compressive strength (UCS, a key indicator of load-bearing capacity) and elastic modulus (E, a measure of material stiffness) of expansive sand paste, and they established a damage model based on acoustic emission parameters that incorporates the loading rate. The development of a damage constitutive model by Dong et al.[28] for freeze-thaw conditions has extended the investigation into aeolian sand backfill performance to more complex operational regimes. Wu et al.[29] developed a power-law creep model to unravel how particle gradation and confining pressure govern the time-dependent deformation of coal gangue backfill, thereby establishing a theoretical basis for forecasting its long-term stability in deep mining.

In conclusion, despite extensive research on the compositional effects, mechanical behavior, and microstructural characteristics of backfill materials, significant variability in material properties persists due to differences in raw materials. Specifically, for aeolian sand backfill, existing studies predominantly focus on single components or fixed curing ages, and a systematic understanding of its mechanical behavior, damage evolution, and energy mechanism under the coupled effects of mass concentration and curing age is still lacking. Therefore, this study investigates the macroscopic mechanical response, energy evolution, and microstructural evolution mechanisms of aeolian sand backfill material through an integrated approach of uniaxial compression tests, acoustic emission (AE) monitoring, and scanning electron microscopy (SEM), with mass concentration (74~80%) and curing age (3~28 days) as the core variables. This research aims to provide a theoretical foundation for optimizing the design and ensuring the safe application of this material in open-pit mine backfilling engineering.

Test system and scheme

Test materials and specimen preparation

The aeolian sand backfill material in this test was prepared using aeolian sand and loess[30,31] as aggregates, whose chemical composition is given in Fig. 1, and a binder consisting of fly ash and P.O. 425 Portland cement. To systematically investigate the coupled effects of mass concentration (a) and curing age (T) on mechanical properties and damage evolution, standard cylindrical specimens (Φ50 mm × 100 mm) were prepared at a values of 74%, 76%, 78% and 80%. Each group of specimens was cured for 3, 7, 14, and 28 days in a standard fog room. After the curing was completed, the end surfaces of specimens were ground flat to ensure uniformity of test loading and data accuracy.

Test scheme

The specimens were placed in an MTS-CMT5305 microcomputer-controlled electronic universal testing machine, with a loading rate of 0.05 mm/min applied until specimen failure, and the uniaxial compression test

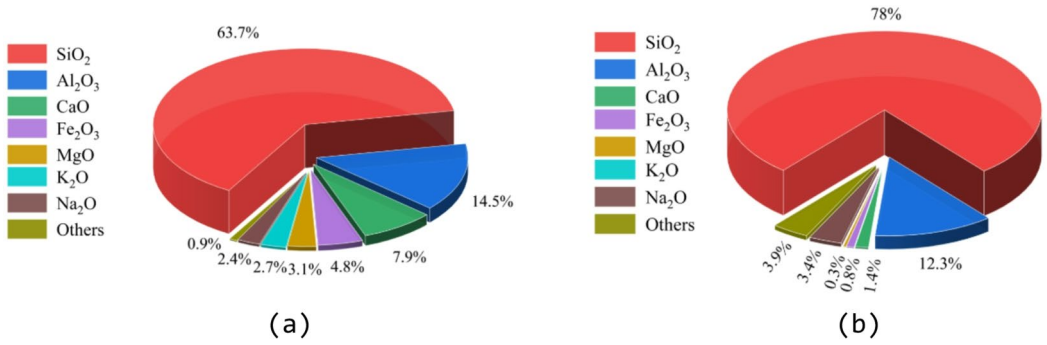

Fig. 1. Chemical compositions of loess and aeolian sand in the open-pit mine area. (**a**) Loess, (**b**) Aeolian sand.

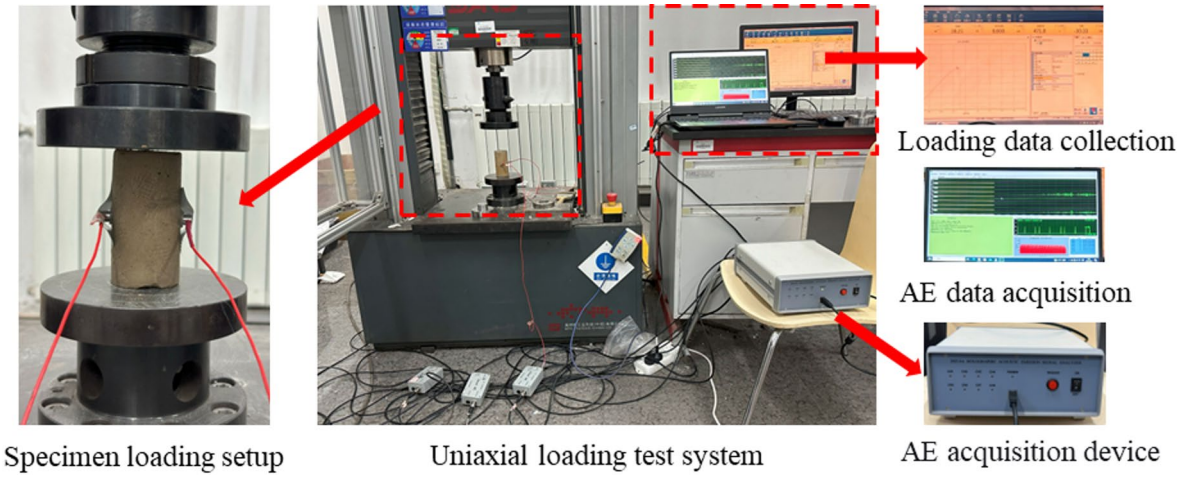

Fig. 2. Uniaxial loading test system.

data were recorded. Simultaneously, the DS5-8 A acoustic emission (AE) monitoring system was employed to monitor AE signals during the compression process. The DS5-8 A system utilizes piezoelectric ceramic transducers as sensors and adopts a dual-transducer configuration to achieve redundant data acquisition, thereby ensuring the completeness and reliability of the AE data. The schematic of the experimental setup is shown in Fig. 2.

Results

Stress–strain curves of backfill under varying mass concentrations and curing ages

Figure 3 shows the stress–strain curves of aeolian sand cemented backfill materials at different curing ages and mass concentrations. Irrespective of the specific a–T combination, all specimens exhibit four characteristic stages: the compaction stage, the linear elastic stage, the yield and peak strength stage, and the post-peak softening failure stage. (1) The initial stage is a non-linear concave-upward region, resulting from the closure of pre-existing micropores. (2) This is followed by an approximately linear-elastic stage, characterized by a linear and steep ascent, indicating a proportional relationship between stress and strain. (3) Subsequently, the curve enters the yield stage, where it deviates from linearity and the slope decreases until the peak stress is reached. (4) Finally, the post-peak stage exhibits strain-softening behavior, characterized by a concave downward shape about the peak as stress decreases with ongoing strain.

Peak stress and elastic modulus of backfill under different mass concentration and curing age

The peak stress (σ_c) and elastic modulus (E) are two core indicators for evaluating the mechanical performance of cemented backfill materials. In this study, uniaxial compression test data of aeolian sand cemented backfill materials were compiled to investigate the influence of mass concentration (a) and curing age (T) on the peak stress and elastic modulus of the backfill.

As shown in Fig. 4, linear functions were employed to fit the variation trends of peak stress and elastic modulus with mass concentration at different curing ages. The fitting coefficients of determination (R^2) all exceed 0.95, indicating that, at a given curing age, both σ_c and E increase linearly with increasing mass concentration. For the 7-day curing age, as a increases from 74% to 80%, the UCS increases from 0.83 MPa to 3.58 MPa, representing a 331.3% enhancement. Similarly, the E rises from 0.18 GPa to 0.43 GPa, representing a comparable

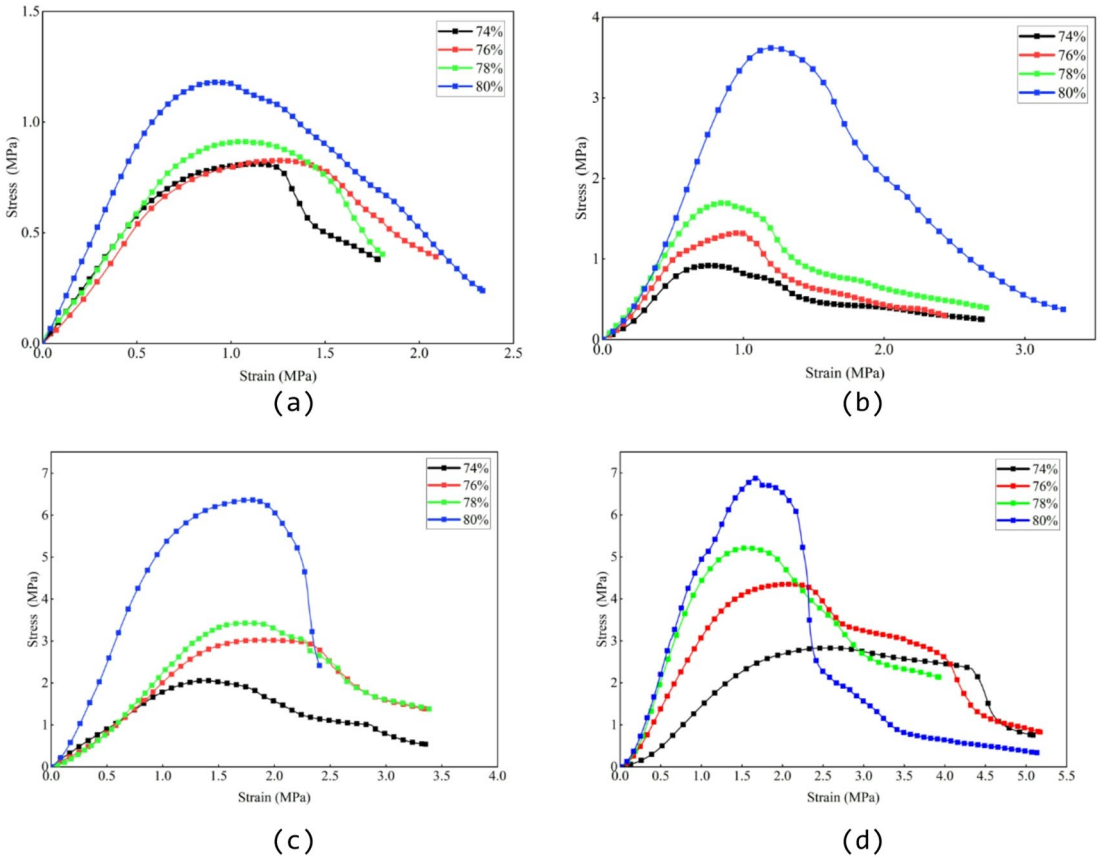

Fig. 3. Stress-strain curves of backfill at different mass concentrations. (**a**) T = 3 days, (**b**) T = 7 days, (**c**) T = 14 days, (**d**) T = 28 days.

increase. Further analysis reveals that the performance gap between different *a* levels widens with curing age. In the low mass concentration range (74%–76%), the increases in strength and modulus are limited across all curing ages. When the mass concentration is increased to 80%, the compressive strengths of the backfill at 3 d, 7 d, 14 d, and 28 d are 1.18 MPa, 3.58 MPa, 6.37 MPa, and 7.01 MPa, respectively. At 14 d, the compressive strength already reaches 6.37 MPa, exhibiting high strength characteristics. This is because the increase in mass concentration raises the proportion of binder (cement and fly ash) in the backfill, leading to an increase in the amount of hydration products. As a result, the aggregate particles in the backfill are more tightly connected, the voids in the backfill structure are effectively filled, and the compactness of the backfill is improved, thereby significantly enhancing its compressive strength. In addition, the hydration reaction of cement is a gradual process, and the pozzolanic reaction of fly ash is typically more active at later curing stages. Therefore, a longer curing age promotes the formation of hydration products such as calcium-silicate-hydrate (C-S-H) gel, enhances the structural stability of the backfill, and consequently improves its compressive strength.

As illustrated in Figs. 5a and c, exponential functions were used to fit the variation trends of σ_c and E_c with curing age under different mass concentrations. All R^2 values are greater than 0.84, demonstrating that, at a constant mass concentration, both σ_c and E_c exhibit an exponential growth trend with increasing curing age. As the curing age extends from 3 to 28 days, σ_c of backfill specimens increases substantially. The values rise from 0.78 to 2.78 MPa, 0.83 to 4.30 MPa, 0.91 to 5.19 MPa, and 1.18 to 7.01 MPa for mass concentrations of 74%, 76%, 78%, and 80%, respectively. Concurrently, E_c values grow from 0.12 to 0.21 GPa, 0.14 to 0.36 GPa, 0.16 to 0.58 GPa, and 0.18 to 0.63 GPa for the corresponding *a* levels. These improvements translate to σ_c increases of 256.4%, 418.08%, 470.33% and 494.07%, and to *E* increases of 75%, 157.14%, 262.5% and 250%, respectively. Figures 5b and d further reveal that the most significant strength gain occurs between 3 and 14 days, particularly for the 80% *a* cohort, which attains σ_c and E_c values of 5.19 MPa and 0.41 GPa at 14 days. Although σ_c and E_c continue to increase from 14 to 28 days, the growth rate decreases. Notably, the 78% *a* group exhibits the highest incremental gain during this late-age period. Collectively, UCS and *E* follow a non-linear, age-hardening trajectory. The 80% *a* specimens outperform all other groups throughout the entire curing period, with the 28-day UCS representing a 494.07% increase over the 3-day value. This reflects a synergistic enhancement effect of high mass concentration combined with adequate curing on the mechanical properties of the backfill.

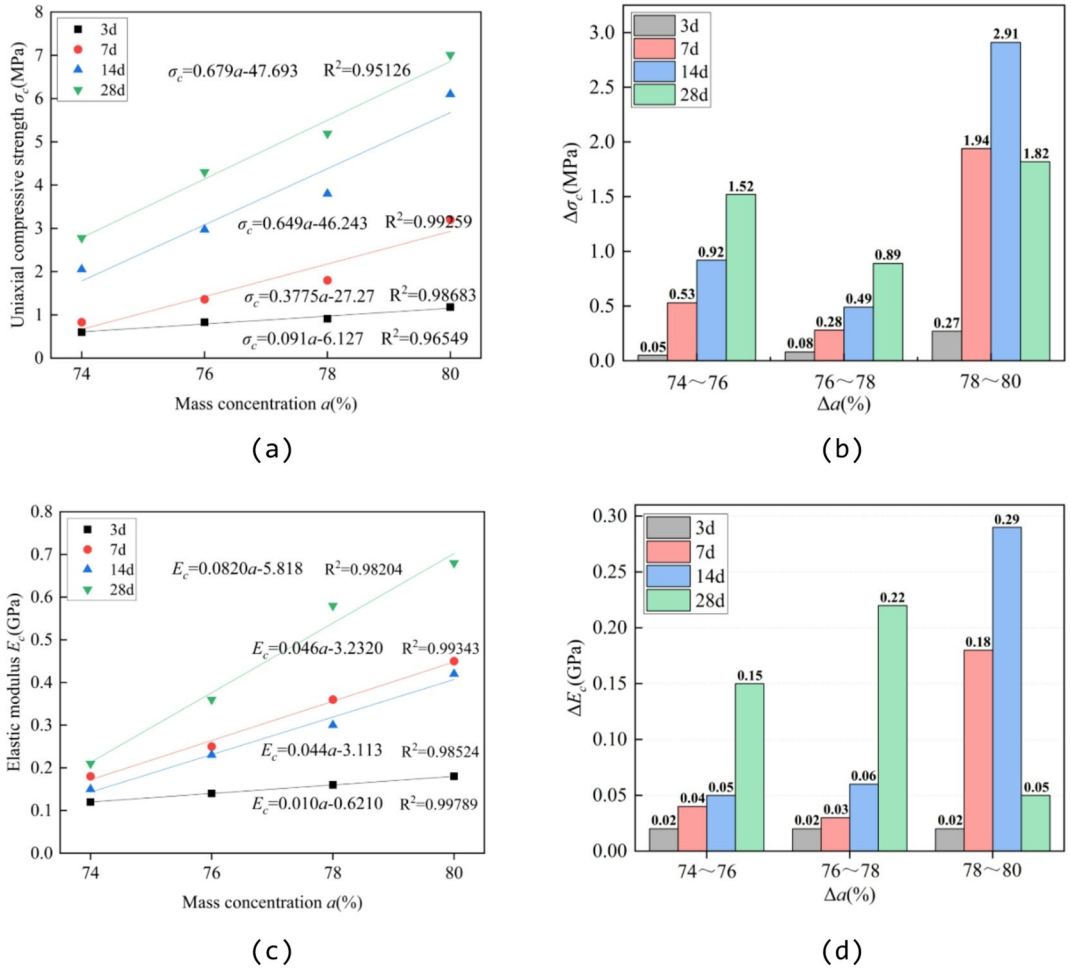

Fig. 4. Effect of mass concentration on the mechanical properties of backfill. (**a**) Variation of σc with a at different curing ages, (**b**) The relationship between Δσc and Δa at different curing ages, (**c**) Variation of Ec with a at different curing ages, (**d**) The relationship between ΔEc and Δa at different curing ages.

Acoustic emission characteristics of backfill materials under different mass concentrations

To further investigate the mechanical properties and damage evolution of aeolian sand cemented backfill, AE characteristics of specimens at different mass concentrations are presented for a curing age of 7 days, as shown in Fig. 6.

Figure 6 shows that the AE characteristics of backfill materials at different mass concentrations correspond to their stress-strain curve features. Irrespective of mass concentration (*a*), AE monitoring indicates that the maximum ringing count consistently occurs near the peak stress. However, the temporal distribution of AE signals evolves with *a*: at lower concentrations, signals are dispersed and fluctuate throughout the loading process, whereas at higher concentrations, they become intensely concentrated and appear as abrupt spikes. Consequently, high *a* specimens exhibit a concentrated energy release near the peak stress, forming high-amplitude ringing counts and leading to more abrupt failure. The maximum ringing count increases linearly from 1.84×10^3 to 3.71×10^3 as the mass concentration was raised from 74% to 80%, representing an increase of approximately 101.63%. These observations demonstrate that the internal structure and failure mechanisms vary significantly with mass concentration at a fixed curing age. The high *a* specimens, characterized by a denser microstructure, lower porosity, and more homogeneous stress distribution, facilitate more complete energy accumulation and concentrated crack propagation, thereby exhibiting distinct brittle failure characteristics.

To further investigate the crack evolution characteristics of the backfill under varying mass concentrations, the crack initiation stress (σ_{CI}) and crack damage stress (σ_{CD}) were determined from the inflection points of the cumulative AE ringing count curves. Quadratic functions were then applied to fit the variation of σ_{CI} and σ_{CD} with mass concentration (*a*), achieving R^2 values above 0.96, as shown in Fig. 7. As the *a* increases from 74% to 80%, σ_{CI} rises linearly from 0.72 MPa to 2.94 MPa and remains consistently within 75%–79% of the corresponding peak stress, indicating a stable micro-crack nucleation threshold. Concurrently, σ_{CD} increases from 0.89 MPa to 3.54 MPa, but its ratio to peak stress decreases slightly from 96.7% to 93.4%. The variations describe above indicate that as *a* increases, the bonding strength of the backfill material enhances and its internal structure becomes denser, leading to increasingly pronounced brittle characteristics. Although crack

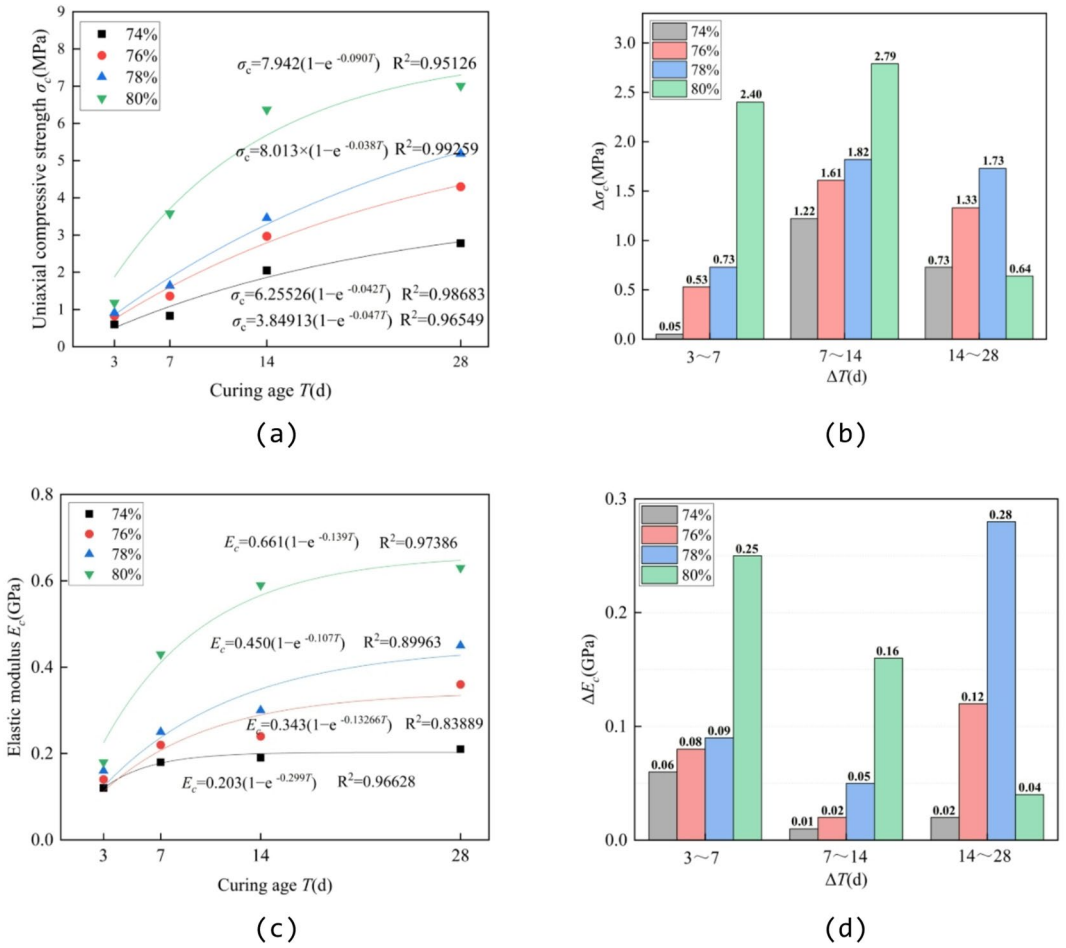

Fig. 5. Effect of curing age on the mechanical properties of backfill. (**a**) Variation of σc with T at different mass concentration conditions, (**b**) The relationship between σc and ΔT at different mass concentration conditions, (**c**) Variation of Ec with T at different mass concentration conditions, (**d**) The relationship between ΔEc and ΔT at different mass concentration conditions.

propagation is delayed before reaching a critical state, concentrated and abrupt failure still occurs as the peak stress is approached. Therefore, while high *a* backfill materials possess greater load-bearing capacity, the failure process involves highly concentrated energy release. This leads to faster and more severe crack penetration, resulting in structural collapse.

Energy evolution characteristics of backfill materials at various mass concentrations

This study investigated the damage evolution mechanism of aeolian sand backfill material using specimens that were cured for 7 days. Based on energy analysis principles, the stress–strain curves were analyzed to reveal the evolution of total energy (U), elastic strain energy (U_e), and dissipated energy (U_d) during loading (Fig. 8). By integrating the slope variation characteristics of the stress-strain curve of the backfill material with the slope inflection points of the cumulative acoustic emission ringing count curve, the characteristic stresses—the crack closure stress (σ_{CC}), the crack initiation stress (σ_{CI}), the crack damage stress (σ_{CD}), and the peak stress (σ_C)—were identified. Accordingly, four characteristic stress points were marked on the curve: A (crack closure), B (crack initiation), C (damage), and D (peak). Based on these points, the energy evolution process was divided into five distinct stages: (I) initial compaction, (II) elastic deformation, (III) stable damage propagation, (IV) peak failure and rapid damage propagation and (V) residual deformation and stabilization.

Table 1 summarizes the energy components at peak strength for 7-day cured backfill at varying mass concentrations. As *a* increases from 74% to 80%, the total energy (U) rises markedly from 0.77 J to 4.45 J, and the elastic strain energy (U_e) grows from 0.41 J to 2.99 J. Consequently, the ratio of elastic energy (U_e/U) increases from 53.25% to 67.19%, indicating a significant enhancement in material stiffness and elastic energy storage capacity. Although the absolute dissipated energy (U_d) also increases, its proportion to the total energy decreases. This trend indicates that higher mass concentrations lead to a more homogeneous microstructure and stronger interfacial bonding within the backfill, which in turn suppresses microcrack propagation and plastic deformation, resulting in a lower proportion of dissipated energy.

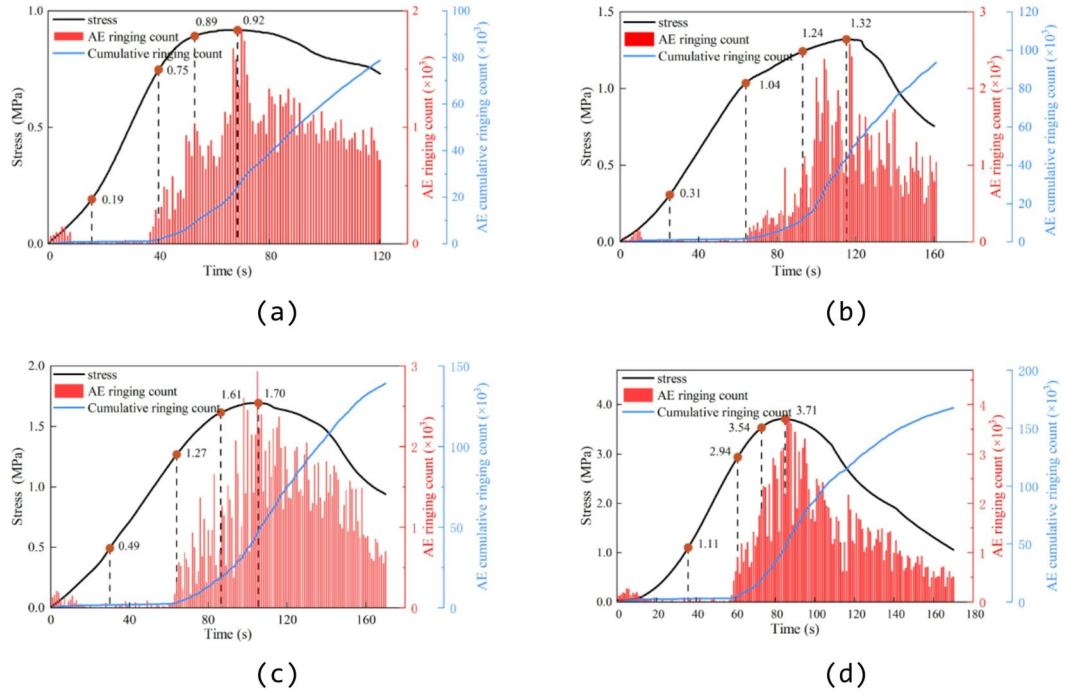

Fig. 6. Influence of *a* on AE ring-down and cumulative counts in backfill during loading. (**a**) T = 7 days, a = 74%, (**b**) T = 7 days, a = 76%, (**c**) T = 7 days, a = 78%, (**d**) T = 7 days, a = 80%.

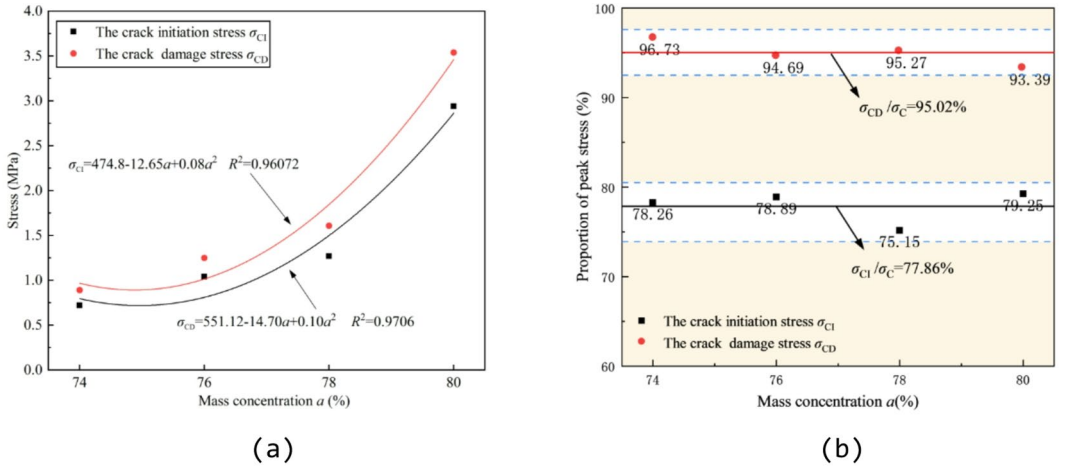

Fig. 7. Relationship between stress and mass concentration of backfill. (**a**) Correlation of σCI and σCD with mass concentration in backfill, (**b**) Correlation of σCI/σC and σCD/σC with mass concentration in backfill.

Additionally, quadratic functions were used to fit the total energy (U), elastic strain energy (U_e), and Dissipated energy (U_d) of the backfill at different mass concentrations, with all R^2 values exceeding 0.92, as presented in Fig. 9. Both U and U_e increase significantly with rising mass concentration (a), reflecting the enhanced overall strength and elastic energy storage capacity of high mass concentration backfill. This phenomenon is primarily attributed to the improved interfacial bonding between binder and aggregate and the increased structural homogeneity. Such microstructural refinement promotes more uniform stress distribution, mitigates local stress concentration, thereby reducing the proportion of energy dissipation and further increasing the ratio of elastic energy.

Microstructure characteristics analysis of backfill materials under different mass concentrations

Taking the 7-day curing age as an example, Fig. 10 illustrates the microstructural morphology of specimens prepared at mass concentrations of 74%, 76%, 78% and 80%. As *a* increases from 74% to 80%, the microstructure

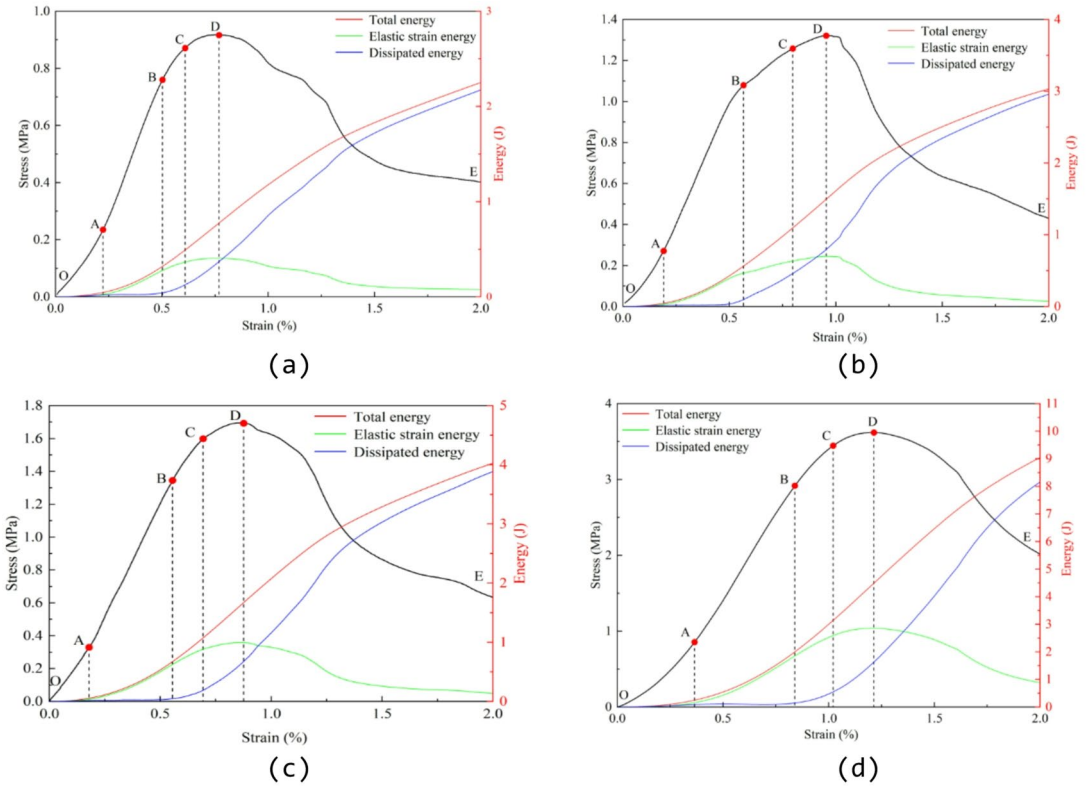

Fig. 8. Evolution of energy characteristics in backfill during loading across a range of *a*. (**a**) T = 7 days, a = 74%, (**b**) T = 7 days, a = 76%, (**c**) T = 7 days, a = 78%, (**d**) T = 7 days, a = 80%.

Mass concentration a(%)	Total energy U(J)	Elastic strain energy U_e(J)	Dissipated energy U_d(J)	The ratio of elastic energy U_e/U
74	0.77	0.41	0.36	53.25%
76	1.48	0.82	0.66	55.41%
78	1.73	1.03	0.7	59.54%
80	4.45	2.99	1.46	67.19%

Table 1. Energy characteristics of cemented backfill at different mass concentrations.

transitions progressively from a loose to a highly compact state. At the lowest concentration (74%), insufficient binder limits the formation of C-S-H gel, resulting in large inter-aggregate pores and a porous matrix. When *a* is raised to 76%, cement hydration intensifies and the micro-filling effect of fly ash is mobilized, which reduces porosity despite the persistence of localized defects. At 78% *a*, hydration approaches completion, and the synergistic interaction between loess and aeolian sand leads to a more homogeneous pore distribution. Upon reaching 80%, abundant hydration products effectively bridge the gaps between aggregates, minimizing porosity and producing a uniformly compact microstructure. Overall, the microstructural evolution can be summarized by the following sequence: an increase in *a* promotes the formation of hydration products, which progressively fill the pores and ultimately lead to structural homogenization.

Discussion

Mechanism of the influence of mass concentration and curing age on the mechanical properties of backfill

The evolution of mechanical performance in aeolian sand backfill is governed by the synergistic effects of mass concentration (*a*) and curing age (*T*). At the microstructural scale, an increase in *a* raises the content of cementitious phases, promoting the formation of hydration products, primarily C-S-H gel. As *a* rises from 74% to 80%, the matrix evolves from a loose, porous framework to a highly compact solid. At lower *a*, insufficient cementitious materials leave pronounced inter-aggregate voids. In contrast, at higher *a*, abundant hydration products effectively infill the inter-particle spaces, markedly reducing porosity and homogenizing the microstructure. A longer curing age (*T*) provides the time required for sustained hydration and, critically, for the secondary pozzolanic reaction of fly ash, which further refines the pore structure and enhances interparticle bonding.

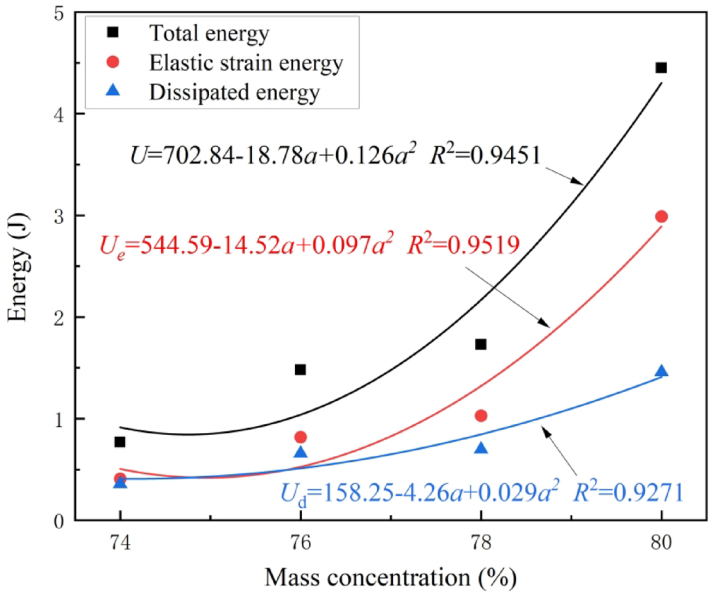

Fig. 9. The influence of mass concentration on various energy values (U, U_e, and U_d).

The refinement in microstructure directly translates to enhanced macroscopic mechanical properties. Both peak stress and elastic modulus increase linearly with a and exponentially with curing age (T). At 80% a and after 28 days of curing, the UCS increases by 494%, accompanied by a significant concurrent increase in elastic modulus. This is attributed to the fact that high-solid-content mixtures provide a more abundant cementing medium, while prolonged curing ensures deeper hydration. The synergy between these factors significantly enhances the stiffness and load-bearing capacity of the backfill.

From an energy evolution perspective, high a specimens exhibit a higher proportion of elastic strain energy (increasing from 53.25% to 67.19%) and more concentrated energy accumulation. AE monitoring shows that high a specimens release energy more abruptly at critical stress states, evidenced by significantly increased ringing counts and a transition in failure mode from plastic to brittle. This behavior indicates that high mass concentration combined with adequate curing promotes structural homogenization. The resulting uniform stress distribution suppresses random microcrack propagation and reduces localized energy dissipation, ultimately leading to failure characterized by substantial energy accumulation and abrupt instability.

In summary, mass concentration (a) primarily governs the potential for mechanical enhancement by increasing the content of cementitious materials and enhancing the initial packing density. Curing age (T), meanwhile, facilitates microstructural densification and interfacial strengthening through sustained hydration reactions. The synergy between a and T leads to a holistic enhancement of aeolian sand backfill properties, resulting in improved performance across multiple scales, from the microstructure to the macroscopic mechanical response.

Mechanism of the influence of mass concentration on crack evolution in backfill

A comprehensive analysis integrating AE monitoring, energy evolution, and stress-strain curves reveals the mechanism by which mass concentration (a) influences the crack evolution behavior of aeolian sand backfill. This influence is characterized by systematic changes in crack initiation, propagation patterns, and failure modes. As a increases from 74% to 80%, the crack evolution shifts from a dispersed and gradual process to a concentrated and abrupt one. At a low a of 74%, the material contains numerous initial pores and exhibits weak cementation. Microcracks initiate at a relatively low stress (σ_{CI} = 0.72 MPa) and propagate from multiple sources. The corresponding AE signals are characterized by low amplitude, dispersed events, and a gradual increase in the ringing count, reflecting progressive crack propagation and coalescence over a large area. This process involves a high proportion of energy dissipation, leading to a failure mode with distinct ductile characteristics.

As a increases, the backfill develops a denser microstructure and more homogeneous cementation. Although the crack initiation stress (σ_{CI}) rises accordingly, its ratio to the peak stress remains stable (75–79%), suggesting a constant threshold for microcrack nucleation. However, upon reaching the crack initiation stress (σ_{CI} = 2.94 MPa), high a (80%) specimens transition rapidly to stable crack propagation. As the stress approaches the crack damage level (σ_{CD} = 3.54 MPa), the AE ring-down count surges abruptly, forming a single high-amplitude peak. This event marks the transition from stable crack growth to unstable macro-crack formation. Concurrently, the proportion of elastic strain energy rises significantly (from 53.25 to 67.19%), indicating that a greater fraction of input energy is stored as elastic deformation. This energy is then concentrated and released abruptly at the critical state, leading to sudden failure.

The coupling between energy evolution and crack propagation reveals that high a backfill exhibits superior elastic energy storage capacity and a lower ratio of dissipated energy. The energy required for crack propagation

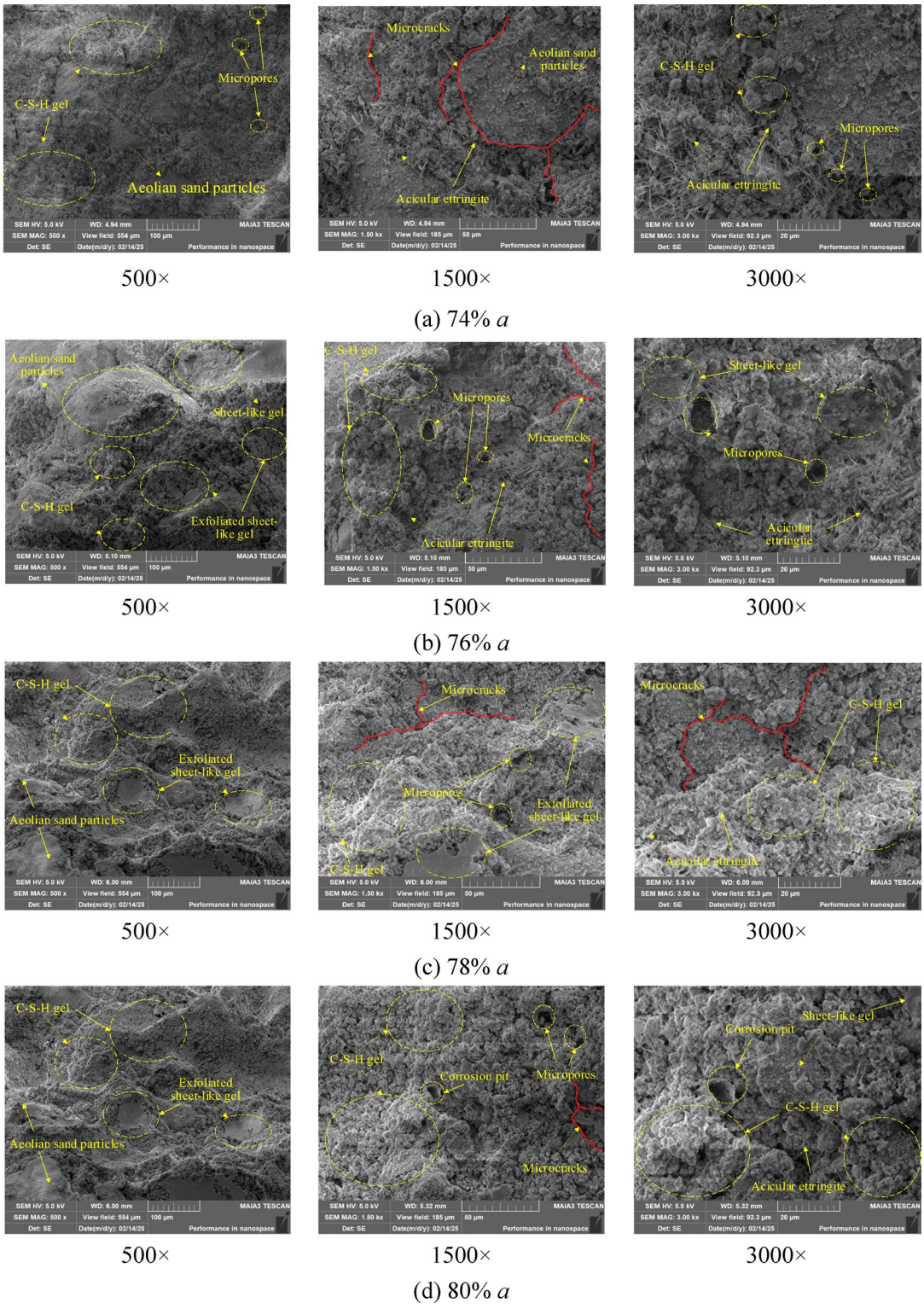

Fig. 10. Microscopic characteristics of aeolian sand backfill. (**a**) 74% a, (**b**) 76% a, (**c**) 78% a, (**d**) 80% a.

primarily originates from the concentrated release of stored elastic strain energy, thereby accelerating crack growth rates and shortening the post-peak stage. Macroscopically, this energy mechanism manifests as a transition from plastic to brittle failure. Furthermore, high *a* specimens maintain significant acoustic emission activity during the post-peak phase, indicating continued crack system evolution after failure. Compared to low *a* specimens, their failure process is notably more rapid and localized.

In summary, mass concentration governs the stress redistribution capacity and energy accumulation-release mechanisms of the backfill by enhancing its structural compactness and uniformity of cementation. This, in

turn, determines the spatial pattern and temporal progression of crack evolution. Increasing concentration shifts the crack behavior from "dispersed initiation–decentralized propagation–progressive failure" to "localized initiation–stable propagation–abrupt instability," exhibiting a distinct ductile-to-brittle transition. This mechanistic understanding provides a critical basis for predicting and controlling the failure behavior of backfill in goaf environments.

Conclusions

This study systematically investigates the mechanical behavior and failure mechanisms of aeolian sand backfill subjected to varying mass concentrations (74%–80%) and curing ages (3–28 d) through uniaxial compression tests. By integrating AE monitoring, energy evolution analysis, and SEM, the work elucidates the coupled relationships among macroscopic mechanical properties, damage evolution, and microstructural development. The key findings are summarized as follows:

(1) Both UCS and E increase linearly with mass concentration (a). As curing age extends from 3 d to 28 d, UCS increases by 256.41%, 418.08%, 470.33%, and 494.07%, while E rises by 75.0%, 157.14%, 262.5%, and 250.0% for backfills with $a = 74\%$, 76%, 78%, and 80%, respectively. These results demonstrate that high a, in synergy with sufficient T, promotes microstructural densification and strengthens interparticle bonding.

(2) AE monitoring reveals a transition in fracture behavior from ductile to brittle with increasing a. At $T = 7$ d, the maximum cumulative AE ring-down count rises linearly from 1.84×10^3 to 3.71×10^3 as a increases from 74 to 80%—an increase of 101.63%. At higher a, AE activity becomes spatially localized and generates high-amplitude events near peak stress, collectively indicating greater energy accumulation, accelerated crack propagation, and more abrupt post-peak failure.

(3) Energy evolution analysis shows that, with increasing a, the backfill stores more total input energy and a higher proportion of elastic strain energy. The elastic strain energy ratio increases from 53.25 to 67.19%, reflecting enhanced elastic energy storage capacity and improved structural homogeneity. This effectively suppresses inelastic deformation and energy dissipation, thereby enhancing the macroscopic stiffness and load-bearing efficiency of the material.

(4) Microstructural analysis confirms that increasing a transforms the internal fabric of the backfill from a loose, porous structure to a homogeneous and compact matrix. This transformation is driven by the increased generation of hydration products, particularly C-S-H gel, which reduces porosity and reinforces interparticle bonding. At $a = 80\%$, a highly dense microstructure develops, accounting for both the superior mechanical performance and the pronounced brittle failure mode.

Data availability

The datasets used and/or analyzed during the current study are available from the corresponding author on reasonable request.

Received: 14 November 2025; Accepted: 20 January 2026
Published online: 27 January 2026

References

1. CAI, Q. & CHEN, Y. Review of 70 years' achievements and high-quality development architecture system of surface coal mining in China. *J. China Coal Soc.* **49**, 235–260 (2024).
2. Jie, D., Xu, X. & Guo, F. The future of coal supply in China based on non-fossil energy development and carbon price strategies. *Energy* **220**, 119644 (2021).
3. Yang, K., Zhao, X., Wei, Z. & Zhang, J. Development overview of paste backfill technology in china's coal mines: A review. *Environ. Sci. Pollut Res.* **28**, 67957–67969 (2021).
4. Hao, J. et al. Synergistic mechanisms of steel Slag, granulated blast furnace slag, and desulfurization gypsum in high-content steel slag-based cementitious backfill materials. *Int. J. Min. Sci. Technol.* **35**, 1005–1018 (2025).
5. Zhao, X. et al. Mix proportion and microscopic characterization of coal-based solid waste backfill material based on response surface methodology and multi-objective decision-making. *Sci. Rep.* **14**, 5672 (2024).
6. Qiao, D. et al. Analysis of the influence of gradation on the strength of a cemented filling body and the cementation strength model. *Integr. Ferroelectr.* **199**, 12–21 (2019).
7. Wu, A., Ruan, Z. & Wang, J. Rheological behavior of paste in metal mines. *Int. J. Min. Metall. Mater.* **29**, 717–726 (2022).
8. Yin, S. et al. A systematic review of paste technology in metal mines for cleaner production in China. *J. Clean. Prod.* **247**, 119590 (2020).
9. Qi, C. & Fourie, A. Cemented paste backfill for mineral tailings management: Review and future perspectives. *Min. Eng.* **144**, 106025 (2019).
10. Sun, Q., Zhang, J. & Zhou, N. Early-Age strength of aeolian Sand-Based cemented backfilling materials: experimental results. *Arab. J. Sci. Eng.* **43**, 1697–1708 (2018).
11. Wang, S., Li, Y., Yang, R., Xu, B. & Lu, B. Rheological behavior with time dependence and fresh slurry liquidity of cemented aeolian sand backfill based on response surface method. *Constr. Build. Mater.* **371**, 130768 (2023).
12. Xin, J. et al. A preliminary study of aeolian sand-cement-modified gasification slag-paste backfill: Fluidity, microstructure, and leaching risks. *Sci. Total Environ.* **830**, 154766 (2022).
13. Zhou, N., Ma, H., Ouyang, S., Germain, D. & Hou, T. Influential factors in transportation and mechanical properties of aeolian sand-based cemented filling material. *Minerals* **9**, 116 (2019).
14. Zhu, L., Zheng, M., Zhang, W., Jing, H. & Ou, Z. Multicomponent cementitious materials optimization, characteristics investigation and reinforcement mechanism analysis of high-performance concrete with full aeolian sand. *J. Build. Eng.* **84**, 108562 (2024).
15. Zhao, Y., Taheri, A., Karakus, M., Chen, Z. & Deng, A. Effects of water Content, water type and temperature on the rheological behaviour of Slag-Cement and fly Ash-Cement paste backfill. *Int. J. Min. Sci. Technol.* **30**, 271–278 (2020).
16. Wang, D., Jiao, D., Cheng, Z., Shi, Q. & Mischo, H. Multi-Criteria comparative analysis of the pressure drop on coal gangue Fly-Ash slurry at different parts along an L-Shaped pipeline. *Int. J. Coal Sci. Technol.* **10**, 28 (2023).

17. Xia, H., Zhang, J., Cai, J., Pan, H. & She, X. Study On the bearing capacity and engineering performance of aeolian sand. *Adv. Mater. Sci. Eng.* **2020**, 3426280 (2020).
18. Ruan, S. et al. Mechanical properties and leaching behavior of modified magnesium slag cemented aeolian sand paste backfill materials. *Constr. Build. Mater.* **387**, 131641 (2023).
19. Zhang, D., Hao, Y., Wen, H., Sun, W. & Zhai, X. Properties optimization and hydration mechanism of Coal-Based solid waste paste filling materials. *Powder Technol.* **455**, 120751 (2025).
20. Wan, Y. et al. Fabrication of eco-friendly mine backfill materials using lead smelting-granulated blast furnace slag-based binder and aeolian sand: Heavy metal leaching behavior and performance design. *Constr. Build. Mater.* **483**, 141655 (2025).
21. Fall, M., Célestin, J. C., Pokharel, M. & Touré, M. A contribution to Understanding the effects of curing temperature on the mechanical properties of mine cemented tailings backfill. *Eng. Geol.* **114**, 397–413 (2010).
22. Zheng, Z., Yang, B., Yang, F., Gu, C. & Liu, H. Experimental investigation into the mechanical and microscopic properties of cemented aeolian sand- coal gangue-fly ash backfill. *Res. Square*. https://doi.org/10.21203/rs.3.rs-3852007/v1 (2024).
23. Wang, D., Yan, H., Qi, C., Lu, S. & Li, B. Study on mechanical properties and damage characteristics of fiber-reinforced ecological-matrix-cemented aeolian sand materials. *Buildings-Basel* **15**, 714 (2025).
24. Hefni, M. A. Investigating the basic properties of basalt fiber reinforced cemented paste backfill as a sustainable material for mine backfilling. *Sci. Rep.* **15**, 10073 (2025).
25. Li, G., Gao, B., Zhu, C., Hu, H. & Fang, H. Study on the deterioration characteristics of aeolian sand concrete under the coupling effect of multiple factors in harsh environments. *PLoS One*. **18**, e0289847 (2023).
26. Hou, Y., Yin, S., Chen, X., Zhang, M. & Yang, S. Study on characteristic stress and energy damage evolution mechanism of cemented tailings backfill under uniaxial compression. *Constr. Build. Mater.* **301**, 124333 (2021).
27. Shao, X. et al. The experimental investigation on mechanics and damage characteristics of the aeolian sand Paste-Like backfill materials based on acoustic emission. *Materials* **15**, 7235 (2022).
28. Dong, W., Shen, X., Xue, H., He, J. & Liu, Y. Research on the freeze-thaw cyclic test and damage model of aeolian sand lightweight aggregate concrete. *Constr. Build. Mater.* **123**, 792–799 (2016).
29. Wu, P. et al. Research on the bearing creep characteristics and constitutive model of gangue filling body. *Sci. Rep.* **14**, 15207 (2024).
30. Lyu, H. et al. Damage evolution laws and constitutive model description of Loess-Slag-Based cemented backfill material. *Constr. Build. Mater.* **495**, 143547 (2025).
31. Lv, H. et al. Performance optimization and characterization of Loess-Slag-Based geopolymer composite: A new sustainable green material for backfill. *Constr. Build. Mater.* **354**, 129103 (2022).

Author contributions

Y. Z. conceived and designed the research. The testing plan was proposed by Y.Z. and G.Z. Material preparation were performed by G.Z. Testing, data collection, and analysis were performed by G.Z., G.Z., H.Z. and X.Z.. The first draft of the manuscript was written by G.Z. and all authors commented on previous versions of the manuscript. All authors read and approved the final manuscript.

Funding

This work was supported by the Xinjiang Uygur Autonomous Region Science and Technology Major Program (No. 2023A01002) and the Ordos major science and technology program (select the best candidates to undertake key research projects) (JBGS-2023-003).

Declarations

Competing interests

The authors declare no competing interests.

Additional information

Correspondence and requests for materials should be addressed to Y.Z.